

Characteristic analysis of 5D symmetric Hamiltonian conservative hyperchaotic system with hidden multiple stability

Li-Lian Huang(黄丽莲), Yan-Hao Ma(马衍昊), and Chuang Li(李创)
Citation: Chin. Phys. B, 2024, 33 (**1**): 010503. DOI: 10.1088/1674-1056/acf9e7
Journal homepage: http://cpb.iphy.ac.cn; http://iopscience.iop.org/cpb

What follows is a list of articles you may be interested in

A discrete Boltzmann model with symmetric velocity discretization for compressible flow

Chuandong Lin(林传栋), Xiaopeng Sun(孙笑朋), Xianli Su(苏咸利),Huilin Lai(赖惠林), and Xiao Fang(方晓)
Chin. Phys. B, 2023, 32 (**11**): 110503. DOI: 10.1088/1674-1056/acea6b

Phase behavior and percolation in an equilibrium system of symmetrically interacting Janus disks on the triangular lattice

Xixian Zhang(张希贤) and Hao Hu(胡皓)
Chin. Phys. B, 2023, 32 (**8**): 080502. DOI: 10.1088/1674-1056/acc7fe

Symmetry phases of asymmetric simple exclusion processes on two lanes with an intersection

Bo Tian(田波), Wan-Qiang Wen(文万强), A-Min Li(李阿敏), and Ping Xia(夏萍)
Chin. Phys. B, 2023, 32 (**7**): 070504. DOI: 10.1088/1674-1056/acc058

Lie symmetry analysis and invariant solutions for the (3+1)-dimensional Virasoro integrable model

Hengchun Hu(胡恒春) and Yaqi Li(李雅琦)
Chin. Phys. B, 2023, 32 (**4**): 040503. DOI: 10.1088/1674-1056/ac9de6

Influence of coupling asymmetry on signal amplification in a three-node motif

Xiaoming Liang(梁晓明), Chao Fang(方超), Xiyun Zhang(张希昀), and Huaping Lü(吕华平)
Chin. Phys. B, 2023, 32 (**1**): 010504. DOI: 10.1088/1674-1056/ac9363

Characteristic analysis of 5D symmetric Hamiltonian conservative hyperchaotic system with hidden multiple stability

Li-Lian Huang(黄丽莲)[1,2,3,†], Yan-Hao Ma(马衍昊)[1,2], and Chuang Li(李创)[1,2]

[1] *College of Information and Communication Engineering, Harbin Engineering University, Harbin* 150001, *China*
[2] *Key Laboratory of Advanced Marine Communication and Information Technology, Ministry of Industry and Information Technology, Harbin Engineering University, Harbin* 150001, *China*
[3] *National Key Laboratory of Underwater Acoustic Technology, Harbin Engineering University, Harbin* 150001, *China*

(Received 5 August 2023; revised manuscript received 12 September 2023; accepted manuscript online 15 September 2023)

Conservative chaotic systems have unique advantages over dissipative chaotic systems in the fields of secure communication and pseudo-random number generator because they do not have attractors but possess good traversal and pseudo-randomness. In this work, a novel five-dimensional (5D) Hamiltonian conservative hyperchaotic system is proposed based on the 5D Euler equation. The proposed system can have different types of coordinate transformations and time reversal symmetries. In this work, Hamilton energy and Casimir energy are analyzed firstly, and it is proved that the new system satisfies Hamilton energy conservation and can generate chaos. Then, the complex dynamic characteristics of the system are demonstrated and the conservatism and chaos characteristics of the system are verified through the correlation analysis methods such as phase diagram, equilibrium point, Lyapunov exponent, bifurcation diagram, and SE complexity. In addition, a detailed analysis of the multistable characteristics of the system reveals that many energy-related coexisting orbits exist. Based on the infinite number of center-type and saddle-type equilibrium points, the dynamic characteristics of the hidden multistability of the system are revealed. Then, the National Institute of Standards and Technology (NIST) test of the new system shows that the chaotic sequence generated by the system has strong pseudo-random. Finally, the circuit simulation and hardware circuit experiment of the system are carried out with Multisim simulation software and digital signal processor (DSP) respectively. The experimental results confirm that the new system has good ergodicity and realizability.

Keywords: Hamilton conservative hyperchaotic system, symmetry, wide parameter range, hide multiple stability

PACS: 05.45.–a, 05.45.Pq **DOI:** 10.1088/1674-1056/acf9e7

1. Introduction

Chaotic systems have the characteristics of ergodicity, pseudo-random, and initial value sensitivity, which make them more suitable for applications in pseudo-random number generators, security communication, and other fields.[1,2] Since Lorenz[3] proposed the first chaotic system in 1963, different types of chaotic systems have been proposed continuously, such as Chen and Ueta's system,[4] Lü and Chen's system,[5] Eisaki *et al.*'s system,[6] and Lü *et al.*'s system.[7] Most of these systems are dissipative systems.[8–12] Conservative systems are an extremely important component of chaos. Compared with dissipative systems, conservative systems have strong specificity. In addition to the characteristics of dissipative chaos, they also have some of their own characteristics. Conservative chaotic systems do not have chaotic attractors,[13–15] but have constant phase volumes and integer dimensions, and are more sensitive to initial conditions, making them more ergodic and pseudo-random. They are more suitable for image encryption than dissipative chaotic systems.[16]

Multi stability is one of many properties of nonlinear dynamic systems.[17,18] It represents the coexistence of different orbits or attractors in a chaotic system while maintaining parameters unchanged and changing initial values, and reflects the influence of initial conditions on the final evolution of the system. This characteristic makes chaotic systems highly flexible in practical applications,[19] It can be applied to processing image or generating different random signal sources for application in the field of information engineering.

The phase space of a conservative chaotic system does not change with time. When the initial space is determined, the phase space cannot be compressed. The dimension of a conservative chaotic system is equal to the dimension of the system, and its trajectory can cross any region in the phase space, while the trajectory of a dissipative chaotic system is confined within the attractive region of attraction because of the existence of attractors, and most of the phase space cannot be reached. Therefore, conservative chaotic systems can produce stronger pseudo-random characteristics, and have inherent advantages in the field of encryption, such as the production of pseudo-random number generators. In 2009, Jia *et al.*[24] proposed a large-scale hyperchaotic system and verified the complexity of the system with analog circuits. In 2013,

[†]Corresponding author. E-mail: lilian_huang@163.com
© 2024 Chinese Physical Society and IOP Publishing Ltd

Liu and Zhang[25] proposed a two-scroll chaotic system with a wide parameter range. In 2019, Xu *et al.*[22] proposed a super large scale chaotic system and carried out adaptive sliding mode control. A wide parameter range chaotic system can keep chaotic state[15] in a wider range, reduce the influence of parameter changes on the system, and stabilize the chaotic characteristics. Therefore, this feature has more advantages in the fields of secure communication,[24] cryptography,[25] chaos control,[22] etc.

Based on the above, this work studies a five-dimensional (5D) Hamiltonian conservative hyperchaotic system with symmetric multi-stability and ultra-wide parameter range. Through the analysis of the constructed conservative hyperchaotic system, it is found that the proposed system has the following characteristics: (i) Hamilton energy and phase volume conservation are satisfied. (ii) It belongs to a conservative hyperchaotic system. (iii) It has an ultra-wide parameter range. (iv) It has hidden dynamics and multistability characteristics. (v) The coexistence of the same and different energy, and the symmetry of these orbits.

In this work, the dynamic characteristics of 5D Hamilton conservative hyperchaotic system are studied through energy analysis, divergence calculation, phase diagram, balance point, Lyapunov index, bifurcation diagram, and SE complexity analysis. It is proved by changing the parameters that the system can maintain chaos and good ergodicity in a wide range of parameters. Then, the multistable characteristics of the system are analyzed in detail, and many energy-related coexisting orbits are found. According to the infinite number of center-type and saddle-type balance points in the system, the hidden chaotic characteristics of the system are illustrated. At the same time, the National Institute of Standards and Technology (NIST) test of the chaotic random sequence generated by the new system in a wide parameter range shows that the pseudo-randomness of the sequence is good, and it is feasible to design the pseudo-random number generator based on the new system. Finally, the circuit simulation and hardware circuit design and implementation of the new system are carried out. The experimental results are consistent with the numerical simulation results, which confirms that the system is a conservative hyperchaotic system with no attractor or superior ergodicity, and it is also realizable.

The rest of this article is arranged as follows. In Section 2, the system modeling and energy analysis are carried out. In Section 3, some basic dynamic characteristics of the system are analyzed. In Section 4, the hidden dynamics and multi-orbital coexistence related to Hamilton energy are given. In Section 5, the SE complexity and NIST test of the system are analyzed. In Section 6, the simulation circuit is built through using the software of mutisim. In Section 7, the hardware is implemented on the DSP platform. Finally, in Section 8, some conclusions are drawn from the present study.

2. System modeling

Euler equation usually describes the motion of a rotating rigid body and can be used to control incompressible fluid.[23] For a rotating rigid body, if the angular velocity of the rigid body is defined as ω and the diagonal matrix of the principal moment of inertia is I, then in the rotating coordinate system, the angular momentum can be expressed as

$$L = \omega \times I. \tag{1}$$

At this point, Γ represents the torque acting on a rigid body, the Newton's law for a rotating system in a spatial coordinate system is called the moment of momentum equation

$$\left(\frac{\mathrm{d}L}{\mathrm{d}t}\right)_S = \Gamma. \tag{2}$$

The momentum equation relationship between the spatial coordinate system and the rotational coordinate system is expressed as

$$\left(\frac{\mathrm{d}L}{\mathrm{d}t}\right)_S = \left(\frac{\mathrm{d}x}{\mathrm{d}t}\right) + \omega \times x. \tag{3}$$

Substituting Γ of Eq. (2) into Eq. (3) for the invariant property of the moment of momentum equation in a rotating coordinate system yields

$$\left(\frac{\mathrm{d}x}{\mathrm{d}t}\right) = \dot{x} = x \times \omega + \Gamma. \tag{4}$$

Equation (4) is the well-known forced rotation Euler rotation equation. When external forces are not considered, the Euler rotation equation of a rotating rigid body is expressed as

$$\dot{x} = x \times \omega = x \times \Pi x, \tag{5}$$

where $x = [x_1, x_2, x_3, x_4, x_5]^{\mathrm{T}}$, $\omega = [\omega_1, \omega_2, \omega_3, \omega_4, \omega_5]^{\mathrm{T}}$, $\Pi = \mathrm{diag}(\Pi_1, \Pi_2, \Pi_3, \Pi_4, \Pi_5)$, and $\Pi_i = I_i^{-1}$ is the reciprocal of the principal moment of inertia, x_i is the angular momentum, and $\omega_i = \Pi_i x_i$ is the angular velocity. The specific form of the system is expressed as

$$\begin{cases} \dot{x}_1 = (\Pi_3 - \Pi_2)\, x_2 x_3, \\ \dot{x}_2 = (\Pi_1 - \Pi_3)\, x_1 x_3, \\ \dot{x}_3 = (\Pi_2 - \Pi_1)\, x_1 x_2, \\ \dot{x}_4 = (\Pi_2 - \Pi_5)\, x_2 x_5, \\ \dot{x}_5 = (\Pi_4 - \Pi_2)\, x_2 x_4. \end{cases} \tag{6}$$

According to the theory of Refs. [26,27], the 5D rigid body Σ is obtained by coupling the sub-rigid body S_{123} and S_{245} on axis 2. The Hamiltonian vector field form of its 5D Euler equation can be described as follows:

$$\Sigma : \dot{x} = J(x)\nabla H(x), \tag{7}$$

where

$$J(\mathrm{x}) = \begin{bmatrix} 0 & -x_3 & x_2 & 0 & 0 \\ x_3 & 0 & -x_1 & -x_5 & x_4 \\ -x_2 & x_1 & 0 & 0 & 0 \\ 0 & x_5 & 0 & 0 & -x_2 \\ 0 & -x_4 & 0 & x_2 & 0 \end{bmatrix}, \tag{8}$$

∇ is the gradient operator, and $H(x)$ is the Hamiltonian energy function and expressed as

$$H(x) = \frac{1}{2}\left(\Pi_1 x_1^2 + \Pi_2 x_2^2 + \prod_3 x_3^2 + \Pi_4 x_4^2 + \Pi_5 x_5^2\right), \tag{9}$$

where $\Pi_i = I_i^{-1}$, I_i is the principal moment of inertia is the moment of inertia of the rigid body, and $\nabla H(x) = [\Pi_1 x_1,\ \Pi_2 x_2,\ \Pi_3 x_3,\ \Pi_4 x_4,\ \Pi_5 x_5]^{\mathrm{T}}$. The system model can be represented as

$$\Sigma : \begin{cases} \dot{x}_1 = (\Pi_3 - \Pi_2) x_2 x_3, \\ \dot{x}_2 = (\Pi_1 - \Pi_3) x_1 x_3 + (\Pi_5 - \Pi_4) x_4 x_5, \\ \dot{x}_3 = (\Pi_2 - \Pi_1) x_1 x_2, \\ \dot{x}_4 = (\Pi_2 - \Pi_5) x_2 x_5, \\ \dot{x}_5 = (\Pi_4 - \Pi_2) x_2 x_4. \end{cases} \tag{10}$$

Since $J(x)$ is a skew symmetric matrix, the differential of Eq. (9) with respect to time is

$$\dot{H}(x) = \nabla H(x)^{\mathrm{T}} \cdot \dot{x} = \nabla H(x)^{\mathrm{T}} J(x) \nabla H(x) = 0. \tag{11}$$

This indicates that the Hamilton energy of system Σ is conservative. The Casimir function is defined as

$$C(x) = \frac{1}{2}(x_1^2 + x_2^2 + x_3^2 + x_4^2 + x_5^2), \tag{12}$$

which satisfies Lie–Poisson brackets. In Eq. (12), $\dot{C} = \{C, H\} = \nabla C(x)^{\mathrm{T}} J(x) \nabla H(x) = 0$.

Therefore, system Σ will not produce chaotic behavior. However, a Hamilton-conservative chaotic system can be obtained by introducing a constant a to destroy the Casimir energy conservation of system Σ and cause the Casimir power to oscillate irregularly. The system Σ^H can be expressed as

$$\Sigma^H : \dot{x} = J^H(x) \nabla H(x), \tag{13}$$

where

$$J^H(x) = \begin{bmatrix} 0 & -x_3 & x_2 & 0 & 0 \\ x_3 & 0 & -x_1 & -x_5 & x_4 \\ -x_2 & x_1 & 0 & a & 0 \\ 0 & x_5 & -a & 0 & -x_2 \\ 0 & -x_4 & 0 & x_2 & 0 \end{bmatrix}, \tag{14}$$

where a is a disturbance parameter, the mathematical model of system Σ^H can be described as

$$\Sigma^H : \begin{cases} \dot{x}_1 = (\Pi_3 - \Pi_2) x_2 x_3, \\ \dot{x}_2 = (\Pi_1 - \Pi_3) x_1 x_3 + (\Pi_5 - \Pi_4) x_4 x_5, \\ \dot{x}_3 = (\Pi_2 - \Pi_1) x_1 x_2 + a\Pi_4 x_2, \\ \dot{x}_4 = (\Pi_2 - \Pi_5) x_2 x_5 - a\Pi_3 x_3, \\ \dot{x}_5 = (\Pi_4 - \Pi_2) x_2 x_4. \end{cases} \tag{15}$$

From Eq. (14), it can be seen that $J^H(x)$ is a skew symmetric matrix, which is substituted into $\dot{H}(x) = \nabla H(x)^{\mathrm{T}} \cdot \dot{x}$ to obtain $\dot{H}(x) = 0$. Therefore, system Σ^H is still conservative in terms of Hamilton energy. The Casimir power of system Σ^H is

$$\begin{aligned} \dot{C}(x) &= \{C, H\} = \nabla C(x)^{\mathrm{T}} J(x) \nabla H(x) \\ &= a(\Pi_4 - \Pi_3) x_3 x_4. \end{aligned} \tag{16}$$

If $a(\Pi_4 - \Pi_3) x_3 x_4 \neq 0$, then the system Σ^H is not a Casimir-conservative system. Set the system parameter $(\Pi_1, \Pi_2, \Pi_3, \Pi_4, \Pi_5) = (14, 20, 10, 5, 30)$, the initial value is $(x_{10}, x_{20}, x_{30}, x_{40}, x_{50}) = (0.5, 0.1, 0.1, 0.1, 0.5)$. When $a = 0$, system Σ^H is the system Σ corresponding to the 5D Euler equation, and both Hamilton energy and Casimir energy are conservative. When $a = 0.7$, the Hamilton energy of system Σ^H is still conservative, but Casimir power begins to oscillate irregularly as shown by the black curve in Fig. 1, the conservative state of Casimir energy is broken. Therefore, system Σ^H is a Hamilton-conservative chaotic system.

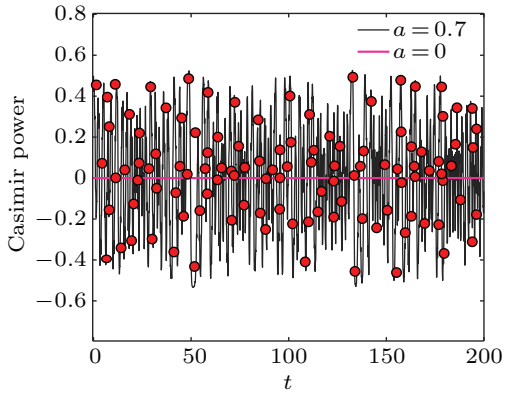


Fig. 1. Time series of Casimir power.

3. Dynamic analysis

3.1. Phase volume conservation

The dissipative characteristics of a system can be determined by the divergence $\nabla \cdot F$. The divergence of the system Σ^H is

$$\nabla \cdot F = \frac{\partial \dot{x}_1}{\partial x_1} + \frac{\partial \dot{x}_2}{\partial x_2} + \frac{\partial \dot{x}_3}{\partial x_3} + \frac{\partial \dot{x}_4}{\partial x_4} + \frac{\partial \dot{x}_5}{\partial x_5} = 0. \tag{17}$$

This indicates that system Σ^H is a conservative system with phase volume conservation.

Conservative systems have no attractors and have strong ergodicity. Phase diagrams are the most direct method of observing the motion state of a system, which can display specific motion trajectories and well illustrate these properties. Set the system parameter to $(\Pi_1, \Pi_2, \Pi_3, \Pi_4, \Pi_5, a) = (14, 20, 10, 5, 30, 0.7)$ and select $(x_{10}, x_{20}, x_{30}, x_{40}, x_{50}) = (0.5, 0.1, 0.1, 0.1, 0.5)$ as the initial value. The partial phase diagram of the system is shown in Fig. 2. It can be seen that the system trajectory presents a chaotic state in the phase space determined by the initial value. The motion trajectory is a spherical closed curve, where there is no chaotic attractor. This once again verifies that the system is a conservative system.

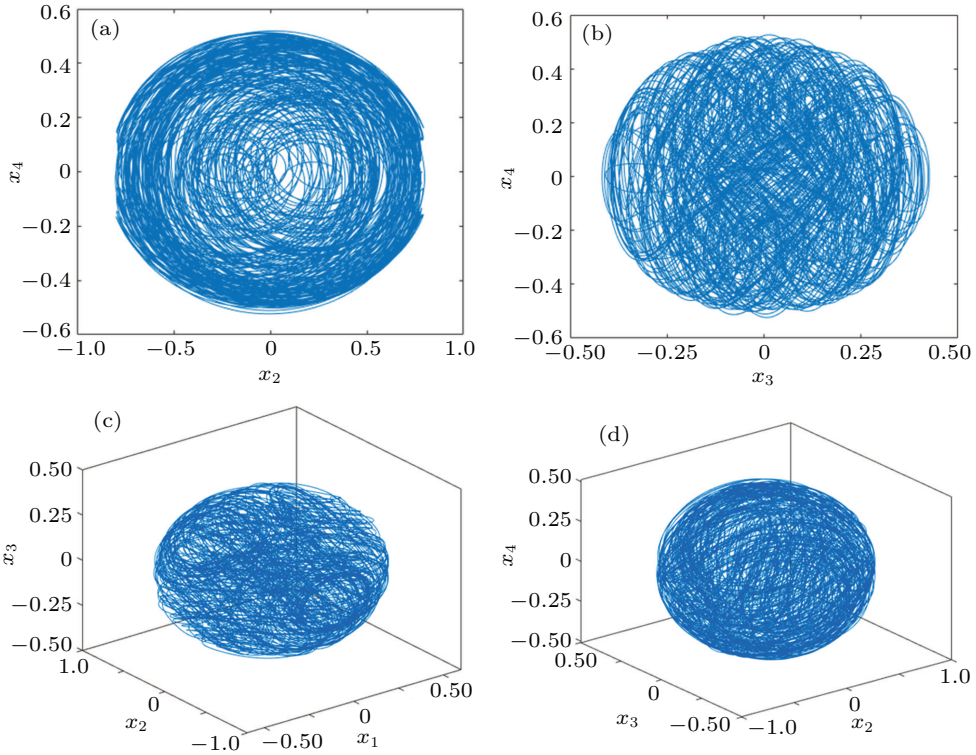


Fig. 2. System phase diagrams: (a) x_2–x_4 plane, (b) x_3–x_4 plane, (c) x_2–x_3–x_4 three-dimensional (3D) space, and (d) x_1–x_2–x_3 3D space.

3.2. Equilibrium point analysis

Equilibrium points play a crucial role in analyzing the properties of a system, which can test whether the system meets the conservative requirements. Owing to the conservation of the phase volume of a conservative system, the system trajectory forms a closed orbit in the phase space determined by the initial value. Therefore, there are no attractors in the system, and there are only two corresponding types of equilibrium points: central type and saddle type.[28] Let $\dot{x}_i = 0$, $i = 1,2,3,4,5$ in Eq. (15), then the following equation (Eq. (18)) can be obtained:

$$\begin{cases} (\Pi_3 - \Pi_2)x_2x_3 = 0, \\ (\Pi_1 - \Pi_3)x_1x_3 + (\Pi_5 - \Pi_4)x_4x_5 = 0, \\ (\Pi_2 - \Pi_1)x_1x_2 + a\Pi_4x_2 = 0, \\ (\Pi_2 - \Pi_5)x_2x_5 - a\Pi_3x_3 = 0, \\ (\Pi_4 - \Pi_2)x_2x_4 = 0. \end{cases} \tag{18}$$

The equilibrium points $(0,0,0,0,0)$, $(l_1,0,0,0,0)$, $(0,l_2,0,0,0)$, $(0,0,0,0,l_5)$, and $(l_1,0,0,0,l_5)$ of the system can be obtained. The new system is linearized at equilibrium point $(x_1^*,x_2^*,x_3^*,x_4^*,x_5^*)$, and the Jacobi matrix is obtained as follows:

$$J_1^H(x) = \begin{bmatrix} 0 & (\Pi_3-\Pi_2)x_3^* & (\Pi_3-\Pi_2)x_2^* & 0 & 0 \\ (\Pi_1-\Pi_3)x_3^* & 0 & (\Pi_1-\Pi_3)x_1^* & (\Pi_5-\Pi_4)x_5^* & (\Pi_5-\Pi_4)x_4^* \\ (\Pi_2-\Pi_1)x_2^* & (\Pi_2-\Pi_1)x_1^* & 0 & a\Pi_4 & 0 \\ 0 & (\Pi_2-\Pi_5)x_5^* & -a\Pi_3 & 0 & (\Pi_2-\Pi_5)x_2^* \\ 0 & (\Pi_4-\Pi_2)x_4^* & 0 & (\Pi_4-\Pi_2)x_2^* & 0 \end{bmatrix}. \tag{19}$$

Substituting $\left|\lambda I - J_1^H(x)\right| = 0$ by the corresponding parameters and equilibrium points yields five characteristic polynomials as follows:

$$f_1(\lambda) = \lambda^3(\lambda^2 + 24.5), \tag{20}$$
$$f_2(\lambda) = \lambda^3(\lambda^2 - 24x_1^2 + 24.5), \tag{21}$$
$$f_3(\lambda) = \lambda(\lambda^4 - 90\lambda^2x_2^2 - 24.5\lambda^2 - 9000x_2^4), \tag{22}$$
$$f_4(\lambda) = \lambda^3(\lambda^2 + 250x_5^2 + 24.5), \tag{23}$$
$$f_5(\lambda) = \lambda^2(\lambda^3 - 24\lambda x_1^2 + 250\lambda x_5^2 + 24.5\lambda + 1190x_1x_5). \tag{24}$$

Let $f_i(\lambda) = 0$, $i = 1,2,3,4,5$, then the corresponding characteristic values will be obtained as shown in Table 1. The three eigenvalues consist of 0 and pure imaginary numbers, and the corresponding equilibrium points belong to the central type, which is consistent with the characteristics of conservative chaotic systems.

Table 1. Equilibrium points and corresponding eigenvalues of system.

Equilibrium points ($l_1 l_3 l_5 \in R$)	Characteristic values ($\sigma\omega \in R^+$)	Equilibrium
$(0,0,0,0,0)$	$(0,0,0,\mathrm{j}\omega,-\mathrm{j}\omega)$	center
$(l_1,0,0,0,0)$	$(0,0,0,\sigma,-\sigma)$	saddle
	$(0,0,0,\mathrm{j}\omega,-\mathrm{j}\omega)$	center
$(0,l_2,0,0,0)$	$(0,\sigma,-\sigma,\sigma,-\sigma)$	saddle
	$(0,\sigma,-\sigma,-\sigma,\sigma)$	saddle
$(0,0,0,0,l_5)$	$(0,0,0,\mathrm{j}\omega,-\mathrm{j}\omega)$	center
$(l_1,0,0,0,l_5)$	$(0,0,\sigma_1,\sigma_2,-\sigma_2)$	saddle
	$(0,0,-\sigma_1,\sigma_2,-\sigma_2)$	saddle
	$(0,0,\sigma,\mathrm{j}\omega,-\mathrm{j}\omega)$	saddle
	$(0,0,-\sigma,\mathrm{j}\omega,-\mathrm{j}\omega)$	saddle

3.3. Symmetry analysis

When the sign of one or more state variables of a system changes and the resulting system is the same as the original system, this means that the system has coordinate transformation symmetry. System Σ^H has the five coordinate transformation symmetries as follows:

$$
\begin{aligned}
&R:(x_1,x_2,x_3,x_4,x_5)\to R:(x_1,-x_2,x_3,-x_4,x_5),\\
&R:(x_1,x_2,x_3,x_4,x_5)\to R:(-x_1,-x_2,x_3,x_4,-x_5),\\
&R:(x_1,x_2,x_3,x_4,x_5)\to R:(x_1,-x_2,-x_3,-x_4,x_5),\\
&R:(x_1,x_2,x_3,x_4,x_5)\to R:(x_1,-x_2,-x_3,x_4,-x_5),\\
&R:(x_1,x_2,x_3,x_4,x_5)\to R:(-x_1,-x_2,x_3,-x_4,-x_5).
\end{aligned}
$$

Time reversal symmetry indicates that the symbol of the state variable changes simultaneously with the change of time transition $t\to -t$, but the transformed system corresponds to the original system.[29,30] Time reversal symmetry is common in conservative systems, but less common in dissipative systems. Time reversal symmetry is crucial in analyzing many physical models.[31,32] System Σ^H has the three types of time reversal symmetry as follows:

$$
\begin{aligned}
&R:(x_1,x_2,x_3,x_4,x_5)\to R:(x_1,-x_2,x_3,-x_4,x_5),\\
&R:(x_1,x_2,x_3,x_4,x_5)\to R:(-x_1,-x_2,x_3,x_4,-x_5),\\
&R:(x_1,x_2,x_3,x_4,x_5)\to R:(x_1,-x_2,-x_3,-x_4,x_5).
\end{aligned}
$$

3.4. Lyapunov exponents and bifurcation diagram analysis

The Lyapunov exponents represent the average exponential divergence rate of the trajectory motion of the system in phase space. When the system is in a chaotic state, at least one of the Lyapunov exponents is positive, which is an important feature in determining whether the system generates chaos. Unlike the scenario in dissipative systems, the Lyapunov exponents of conservative chaotic systems have symmetry, and their sum is zero. According to the set parameters, the Lyapunov exponents of the system are calculated by using the Wolf method,[33] and obtain $LE_{12345} = [1.13282, 0.01284, -0.00259, -0.01219, -1.13088]^{\mathrm{T}}$, $LE_S = 0$.

In 1983, Kaplan Yorke put forward the Lyapunov dimension[34] to determine the types of attractors in dynamic systems. The dimension of strange attractor must be lower than the dimension of the space of dynamic system. However, owing to the absence of strange attractors in conservative chaotic system, the Lyapunov dimension must be equal to the dimension of dynamic system. The Lyapunov dimension of system Σ^H is

$$
D_{\mathrm{L}} = 4 + \frac{LE_1 + LE_2 + LE_3 + LE_4}{|LE_5|} = 5. \tag{25}
$$

Therefore, the Lyapunov dimension is the same as the system dimension, which is consistent with the definition that a conservative system does not have an attractor, and the sum of the Lyapunov exponents is 0, which proves that the phase space of the system does not change.

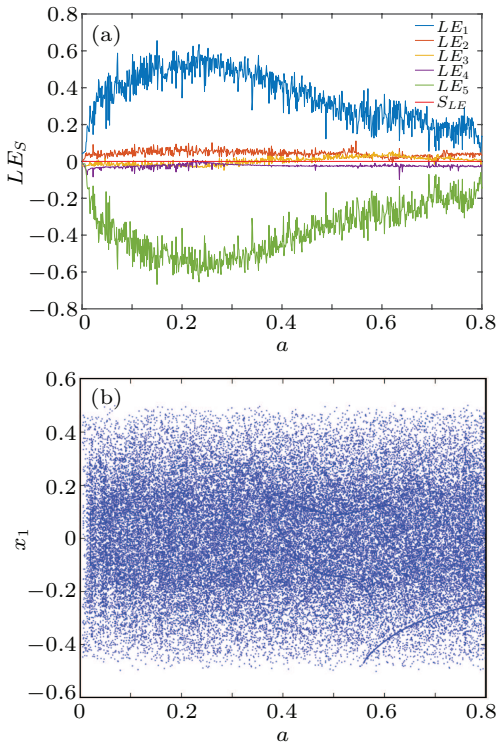


Fig. 3. (a) Lyapunov exponents and (b) bifurcation diagram of the system Σ^H.

Figure 3(a) shows the Lyapunov exponents spectrum of the system as it changes with parameter a. It can be seen that the Lyapunov exponents are symmetric about 0, with two curves significantly larger than 0, and the middle curve basically coincides with the x axis, proving that the system is a 5D conservative hyperchaotic system. The corresponding bifurcation diagram is shown in Fig. 3(b). Unlike dissipative chaotic systems, the conservative system almost immediately enters a hyperchaotic state when the parameter a is set to be larger than 0, i.e., $a > 0$. This is because the conservative system has no attractors, and the initial conditions of the system are located in the hyperchaotic region.

3.5. Analysis of wide parameter range

The most obvious advantage of a system with an wide parameter range is its high stability, which allows the parameters to change in a wide range while the chaotic state keeps unchanged, which means that the system can maintain good chaotic characteristics without state decay in this wide range.

The wide Lyapunov exponents and bifurcation diagram of the system with respect to parameters are given below to prove the existence of wide parameter range. Set parameters $(\Pi_1,\Pi_2,\Pi_3,\Pi_4,\Pi_5,a)=(14,20,10,5,30,0.7)$, initial value selection $(x_{10},x_{20},x_{30},x_{40},x_{50})=(0.5,0.1,0.1,0.1,0.5)$. When the parameter Π_2 changes within the interval $[-7000,7000]$, the Lyapunov exponents spectrum of the system is shown in Fig. 4(a). It can be seen that the first curve is always greater than zero, which proves that the system has been in chaotic state. Figure 4(b) shows the bifurcation diagram, which is a verification of Lyapunov exponents.

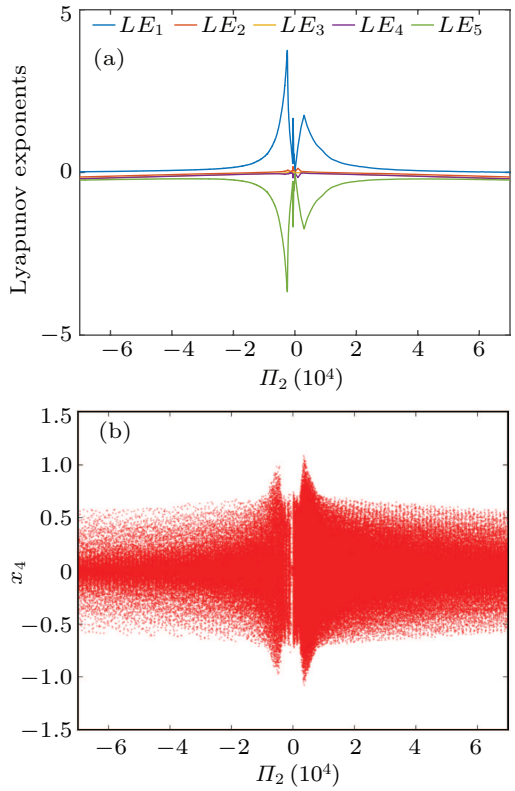


Fig. 4. (a) Lyapunov exponents and (b) bifurcation diagram varying with Π_2.

4. Hidden dynamics and multiple stability analysis

In the dissipative chaotic system, without changing the system parameters, the system presents a variety of phase trajectories of different positions or topological structures with the change of initial conditions, which is called the coexistence of multiple attractors. This phenomenon is also known as multiple stability.

4.1. Hidden dynamics analysis with Hamiltonian energy in HCCS

Hidden attractors have been found in many dissipative systems, such as dissipative systems with only stable equilibrium points, dissipative systems without equilibrium points, and dissipative systems with infinite equilibrium points,[35–37] which are shown in Table 1. System Σ^H has only two types of equilibrium points: central type and saddle type, but system Σ^H has infinite equilibrium points, so system Σ^H should have hidden chaotic attractors. However, there is no attractor in a conservative system, so this kind of chaos is not a hidden attractor, but is considered as a conservative hidden chaotic orbit.

Set the system parameter to $(\Pi_1,\Pi_2,\Pi_3,\Pi_4,\Pi_5,a)=(14,20,10,5,30,0.7)$ by changing the initial value x_{10} of system state variable x_1, the bifurcation diagram and corresponding Lyapunov exponents spectrum shown in Fig. 5 are obtained. It can be seen from Fig. 5(a) that the bifurcation diagram of system Σ^H in the range of initial value $x_{10}\in(-0.21,0.19)$ forms a narrow band, indicating that the system is in quasi-periodic state in this range, which can be verified by the Lyapunov exponents in Fig. 5(b).

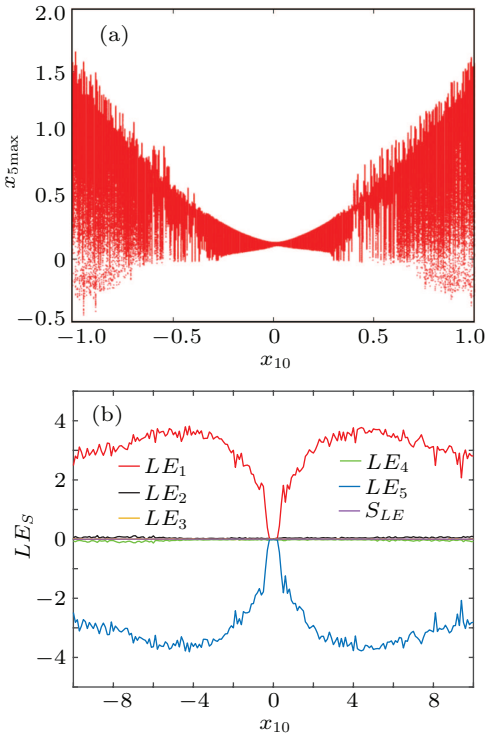


Fig. 5. (a) Bifurcation diagram and (b) Lyapunov exponents varying with x_{10}.

In order to illustrate the influence of Hamilton energy on hidden dynamics, in Fig. 6, the spatial distributions of Hamilton energy in the initial plane of x_{10}–x_{20} and x_{40}–x_{50} are plotted, with color bars representing the Hamilton energy values. It can be seen from the figure that with the increase of the initial value of the system, the Hamiltonian energy increases

correspondingly. When the initial value is small, the system undergoes quasi-periodic motion and weak chaotic motion at relatively low energy. With the increase of energy, these motions gradually enter into chaotic states.

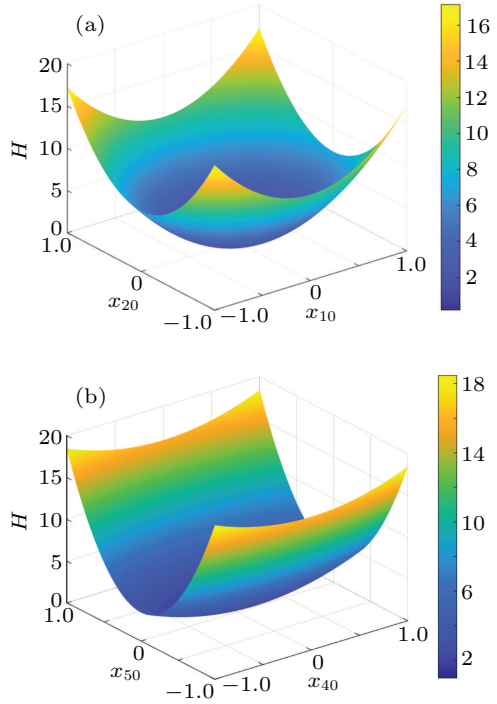


Fig. 6. Hamilton energy spatial distribution diagram in (a) x_{10}–x_{20} plane and (b) x_{40}–x_{50} plane.

For Figs. 6(a) and 6(b), the Hamilton energy expressions of the system are respectively written as

$$H = \frac{1}{2}\sum_{i=1}^{4} \Pi_i x_i^2 = \frac{1}{2}(14x_{10}^2 + 20x_{10}^2 + 4.65), \quad (26)$$

$$H = \frac{1}{2}\sum_{i=1}^{4} \Pi_i x_i^2 = \frac{1}{2}(5x_{40}^2 + 30x_{50}^2 + 3.8). \quad (27)$$

In general, orange in Fig. 6 corresponds to strong chaotic orbits, and dark blue refers to quasi-periodic or weak chaotic orbits. Therefore, the change trend of dynamic behavior can be intuitively reflected through Hamilton energy diagram.

4.2. Equal-energy orbit coexistence

Casimir power determines whether system Σ^H forms a chaotic orbit. When Casimir energy is not conserved, Hamilton energy will affect the coexistence behavior of the system. From the bifurcation diagram and Lyapunov exponents in Fig. 5, it can be seen that system Σ^H is multi-stable. On this basis, by changing the sign of the initial value of the system, the system orbit with the same Hamilton energy can be obtained.

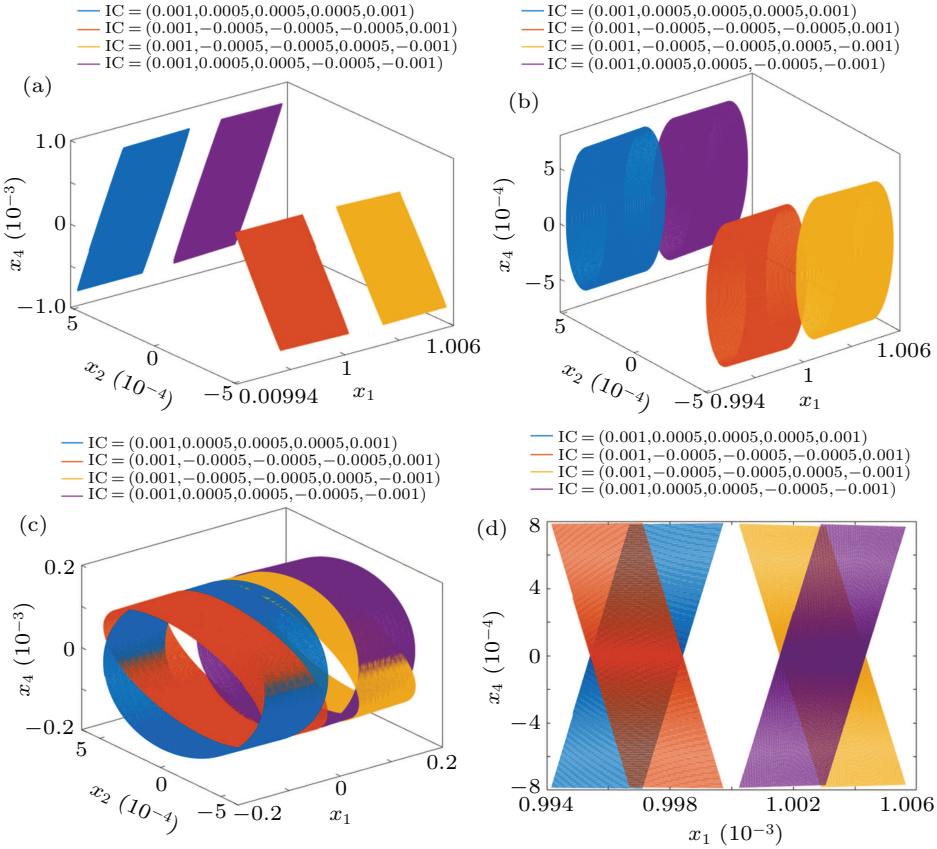


Fig. 7. Phase diagram of system Σ^H with Hamilton energy of 5.275×10^{-5} in (a) x_1–x_2–x_4 three-dimensional (3D) space, (b) x_1–x_2–x_3 3D space, (c) x_1–x_3–x_4 3D space, and (d) x_1–x_4 plane.

In this way, under the same Hamilton energy, different initial values will produce different orbits. To illustrate this point in detail, Hamilton energy is selected in these three cases. It can be found that the system Σ^H corresponds to the coexistence of

quasi periodic orbits with low Hamilton energy, as shown in Fig. 7. It should be noted that these orbits are all symmetrical. As the Hamilton energy transitions to a higher value, the system exhibits coexistence of quasi periodic orbits and weak chaotic orbits as shown in Fig. 8. As Hamilton energy continues to increase, chaotic orbits coexist in system Σ^H as shown in Fig. 9, which are also symmetrical. This is very rare in conservative chaotic systems.

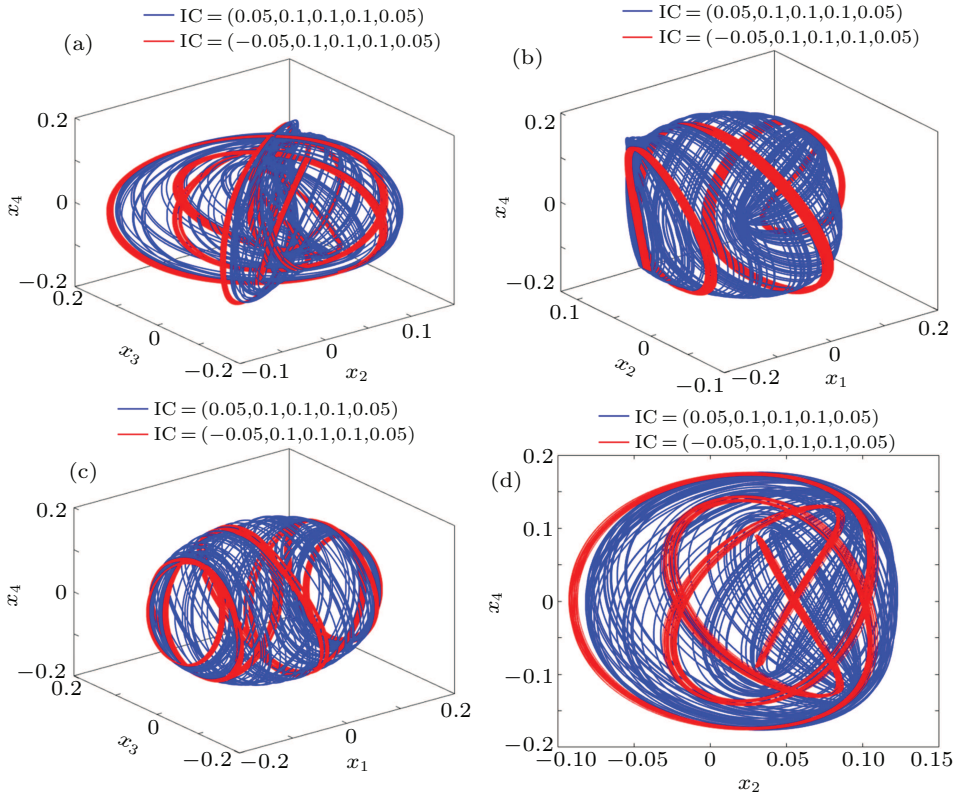


Fig. 8. Phase diagram of system Σ^H with Hamilton energy of 0.23 in (a) x_2–x_3–x_4 3D space, (b) x_1–x_2–x_4 3D space, (c) x_1–x_3–x_4 3D space, and (d) x_2–x_4 plane.

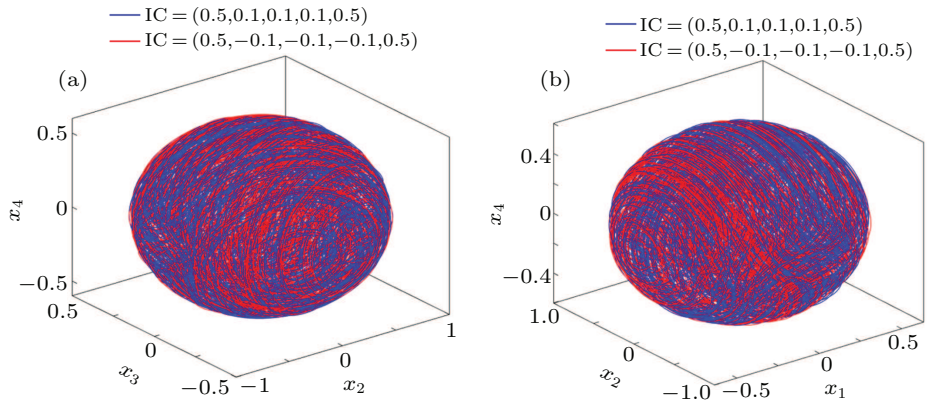


Fig. 9. Phase diagram of system Σ^H with Hamilton energy of 5.675 in (a) x_2–x_3–x_4 3D space, and (b) x_1–x_2–x_4 3D space.

4.3. Different energy orbit coexistence

Through research, it is found that system Σ^H not only has orbital coexistence with the same energy, but also has orbital coexistence behavior with unequal energy at different initial values. Set the system parameter to $(\Pi_1, \Pi_2, \Pi_3, \Pi_4\Pi_5, a) = (14, 20, 10, 5, 30, 0.7)$, and set the initial values of x_{10} in system Σ^H to 0.5, 2.5, and 5 in sequence, while keeping other initial values unchanged. From the figure, it can be seen that different initial values of energy can lead the orbits of different sizes to coexist. The higher the energy, the larger the volume occupied by the system orbit is and the stronger the ergodicity. Figure 10(b) shows the corresponding timing diagram. It can be seen that with the increase of x_{10}, the amplitude of the time domain waveform increases, indicating that the chaos and randomness of system Σ^H are enhanced.

Attraction basins can intuitively reflect the phase trajectory of coexistence. Figure 11 shows the local suction basin of system Σ^H in the x_3–x_4 plane when the parameter is $(\Pi_1, \Pi_2, \Pi_3, \Pi_4, \Pi_5, a) = (14, 20, 10, 5, 30, 0.7)$ and the initial value is $(x_{10}, x_{20}, x_{30}, x_{40}, x_{50}) = (0.5, 0.1, 0.1, 0.1, 0.5)$. It

can be found that the attraction basin has a circular structure, where different colors represent different types or amplitude of phase trajectories. Therefore, there are very rich coexistence behaviors in this system.

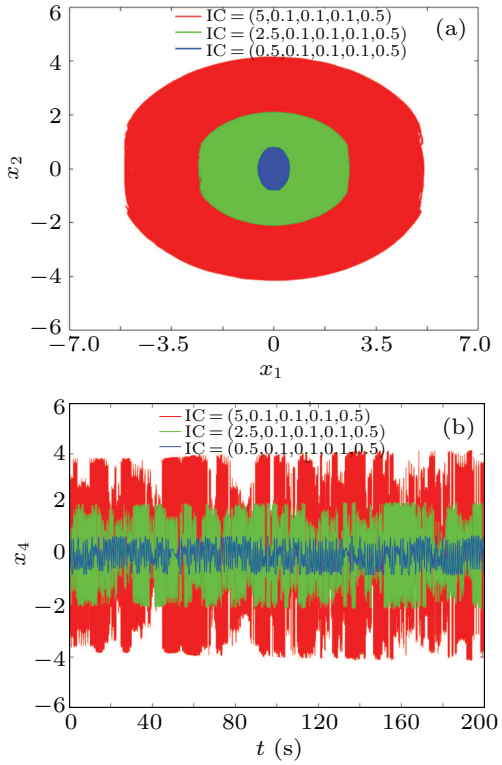


Fig. 10. Phase diagrams and time series of Casimir power: (a) x_1–x_2 plane phase diagrams when the initial value x_{10} is different, and (b) time series diagram when the initial values of x_{10} are different.

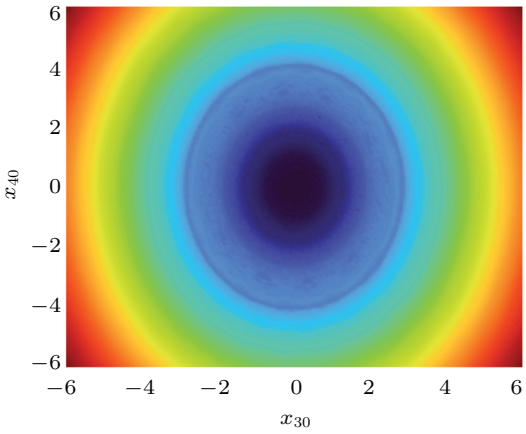


Fig. 11. Local basin of attraction in x_{30}–x_{40} plane.

5. SE complexity analysis

Complexity testing is an important method to analyze the complexity of chaotic system. The complexity of a chaotic system refers to the ability of the system to generate random sequences by using relevant algorithms. In this work, the SE complexity algorithm with high accuracy and high speed is used for analysis. The SE algorithm uses the energy distribution in the Fourier transform domain and the corresponding SE value is obtained based on the Shannon entropy algorithm.[38] The larger the SE value, the higher the complexity of the system is and the stronger the randomness of the generated sequence.

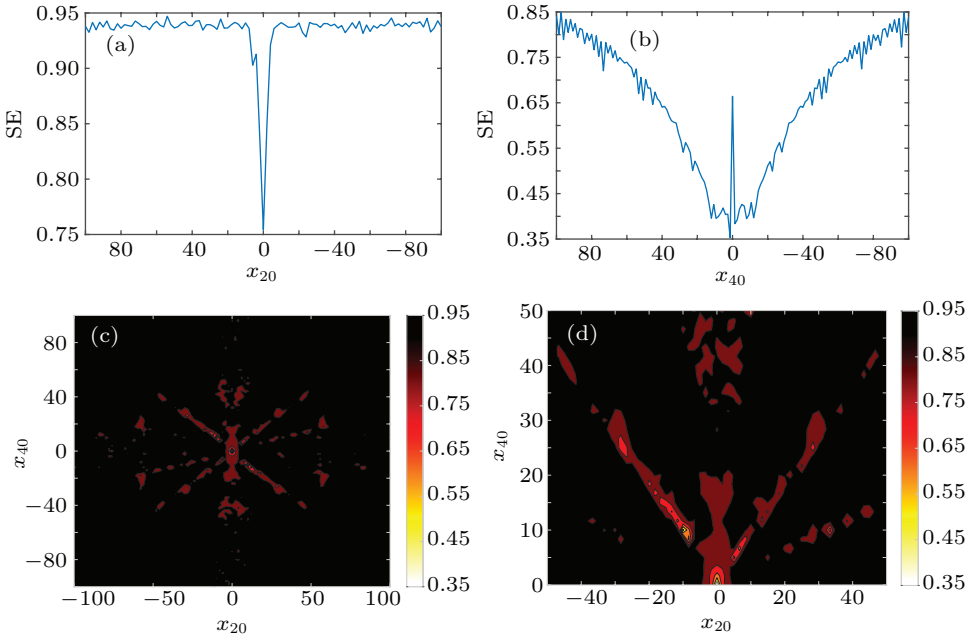


Fig. 12. SE complexity changing with initial value (a) x_{20} and (b) x_{40}, SE complexity map of the system with two initial values change (c) $x_{20}, x_{40} \in [-100, 100]$, and (d) $x_{20} \in [-50, 50], x_{40} \in [0, 50]$.

In order to better describe the influence of initial value change on the complexity of the new system, in this section the SE complexity tests on the two initial values of the new system are conducted, and the test results are shown in Figs. 12(a) and 12(b). In addition, the chaos diagram of SE complexity is also drawn based on two initial value changes. As can be seen from Figs. 12(c) and 12(d), the parameter $(\Pi_1, \Pi_2, \Pi_3, \Pi_4, \Pi_5, a) = (14, 20, 10, 5, 30, 0.7)$ and

initial value $(x_{10}, x_{30}, x_{50}) = (0.5, 0.1, 0.5)$ fluctuate in complexity near the coordinates (0,0), while most of other regions have high complexity above 0.9. Fixed $x_{20} = 0$, it can be found that the trend of x_{40} is consistent with the SE complexity in Fig. 12(b), and has a certain degree of symmetry. Similarly, by fixing $x_{40} = 0$, it can be found that the change trend of x_{20} is consistent with the SE complexity in Fig. 12(a). It is proved that the new system has multiple stability phenomena with high complexity.

5.1. NIST testing

The NIST test[39] is an effective tool for detecting random sequences, which can examine the degree of deviation of the statistical characteristics of the tested sequence from the ideal random sequence from different perspectives. It includes 15 test items. Each test will receive a P-value value. The randomness of the sequence is determined by judging the P-value of each term. To satisfy the requirements, NIST testing needs to meet the following three indicators:

(i) The P-value of each test item must be greater than or equal to the significance level $\alpha = 0.01$.

(ii) The sequence test pass rate must be within a confidence interval of $(\hat{p} - 3\sqrt{\hat{p}(1-\hat{p})/m}\hat{p} + 3\sqrt{\hat{p}(1-\hat{p})/m})$, where $\hat{p} = 1 - \alpha$, $m = 100$ is the number of the test sequences, and the corresponding confidence interval is (0.9602,1.0198).

(iii) The P-value value conforms with a uniform distribution.

In the test, set the parameter $(\Pi_1, \Pi_2, \Pi_3, \Pi_4, \Pi_5, a) = (14, 20, 10, 5, 30, 0.7)$ of system Σ^H with an initial value of $(x_{10}, x_{20}, x_{30}, x_{40}, x_{50}) = (0.5, 0.1, 0.1, 0.1, 0.5)$, and the test results are shown in Table 2. From the table, it can be seen that all P values obtained in the statistical test are greater than the significance level $\alpha = 0.01$, and the pass rates of each test are within the confidence interval. In addition, histogram is also used to test the uniformity of the distribution of P values. In order to fully reflect the uniformity of the P-values distribution, we select the non overlapping module matching test with the most testing times for histogram verification. As shown in Fig. 13, it can be seen that the distribution of P values in the system has good uniformity.

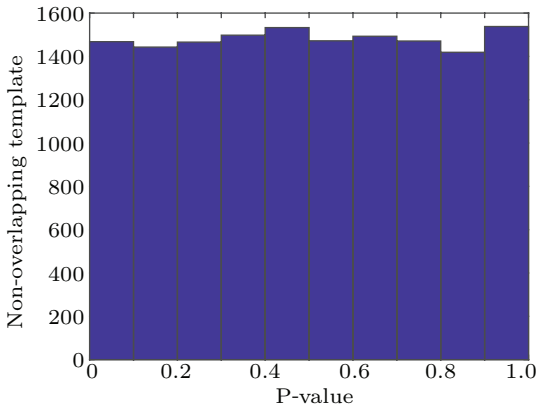


Fig. 13. P-value histogram of non-overlapping template matching test of system Σ^H.

In summary, the chaotic sequences generated by this system have good pseudo-random characteristics, and can be applied to the design of pseudo-random signal generators.

Table 2. NIST test results.

No.	Randomness test	P-value	Proportion
1	frequency	0.759756	0.99
2	block frequency	0.616305	1
3	runs	0.699313	1
4	longest run of one's	0.262249	0.98
5	matrix rank	0.834308	0.99
6	FFT	0.042808	0.97
7	non-overlapping template	0.978072	1
8	overlapping template	0.935716	0.99
9	universal	0.236810	0.98
10	linear complexity	0.779188	1
11	serial test	0.023545	0.99
12	approximate entropy	0.798139	0.98
13	cumulative sums test	0.834308	0.99
14	random excursions	0.739918	1
15	random excursions variant	0.883171	0.99

6. Multisim circuit simulation design and implementation

In this section, the analog circuit of the conservative hyperchaotic system is designed and physically implemented using linear resistors, linear capacitors, multipliers, and operational amplifiers with different resistance values. Substituting parameters $(\Pi_1, \Pi_2, \Pi_3, \Pi_4, \Pi_5, a) = (14, 20, 10, 5, 30, 0.7)$ into Eq. (15) yields

$$\begin{cases} \dfrac{\mathrm{d}x_1}{\mathrm{d}t} = -10x_2x_3, \\ \dfrac{\mathrm{d}x_2}{\mathrm{d}t} = 4x_1x_3 + 25x_4x_5, \\ \dfrac{\mathrm{d}x_3}{\mathrm{d}t} = 6x_1x_2 + 3.5x_4, \\ \dfrac{\mathrm{d}x_4}{\mathrm{d}t} = -10x_2x_5 - 7x_3, \\ \dfrac{\mathrm{d}x_5}{\mathrm{d}t} = -15x_2x_4. \end{cases} \tag{28}$$

The proposal of Eq. (28) conduces to designing and optimizing circuit systems, and its contribution lies in the ability to simulate the behavior of the entire circuit system and verify the correctness and performance of the design by establishing system equations and combining it with the simulation function of multisim. Its motivation is to achieve modular design of circuits, further deriving corresponding circuit state equations, analyzing the circuit system as a whole, better understanding the working principle and overall performance of the circuit system, revealing the interactions between different components, analyzing their influences on system behavior, and more comprehensively describing and analyzing the behavior and performance of the entire circuit system. This helps to better understand and optimize circuit systems, ensuring system stability, and meeting performance requirements.

Let the Hamiltonian energy function of a dimensionless dynamic system (28) be $H_*(x)$, then, according to the Helmholtz theorem, the change in energy will come from the work done by the force field. The energy function $H_*(x)$ satisfies the following conditions:

$$\begin{cases} \nabla H(x)_*^{\mathrm{T}} F_{\mathrm{c}}(x) = 0, \\ \nabla H(x)_*^{\mathrm{T}} F_{\mathrm{d}}(x) = \dot{H}_*(x) = \dfrac{\mathrm{d}H(x)_*}{\mathrm{d}t}, \end{cases} \tag{29}$$

where

$$\nabla H_*^{\mathrm{T}}(x) = \left[\frac{\partial H(x)_*}{\partial x_1} \quad \frac{\partial H(x)_*}{\partial x_2} \quad \frac{\partial H(x)_*}{\partial x_3} \quad \frac{\partial H(x)_*}{\partial x_4} \quad \frac{\partial H(x)_*}{\partial x_5} \right],$$

gradient field and vortex field are

$$F_{\mathrm{c}}(x) = \begin{bmatrix} 0 & \dfrac{\partial F_1(x)}{\partial x_2} & \cdots & \dfrac{\partial F_1(x)}{\partial x_n} \\ \dfrac{\partial F_2(x)}{\partial x_1} & 0 & \cdots & \dfrac{\partial F_2(x)}{\partial x_n} \\ \vdots & \vdots & & \vdots \\ \dfrac{\partial F_n(x)}{\partial x_1} & \dfrac{\partial F_n(x)}{\partial x_2} & \cdots & 0 \end{bmatrix} \begin{bmatrix} x_1 \\ x_2 \\ \vdots \\ x_n \end{bmatrix}, \tag{30}$$

$$F_{\mathrm{d}}(x) = \begin{bmatrix} \dfrac{\partial F_1(x)}{\partial x_1} & 0 & \cdots & 0 \\ 0 & \dfrac{\partial F_2(x)}{\partial x_2} & \cdots & 0 \\ \vdots & \vdots & & \vdots \\ 0 & \cdots & \cdots & \dfrac{\partial F_n(x)}{\partial x_n} \end{bmatrix} \begin{bmatrix} x_1 \\ x_2 \\ \vdots \\ x_n \end{bmatrix}. \tag{31}$$

The matrix equation corresponding to Eq. (28) is

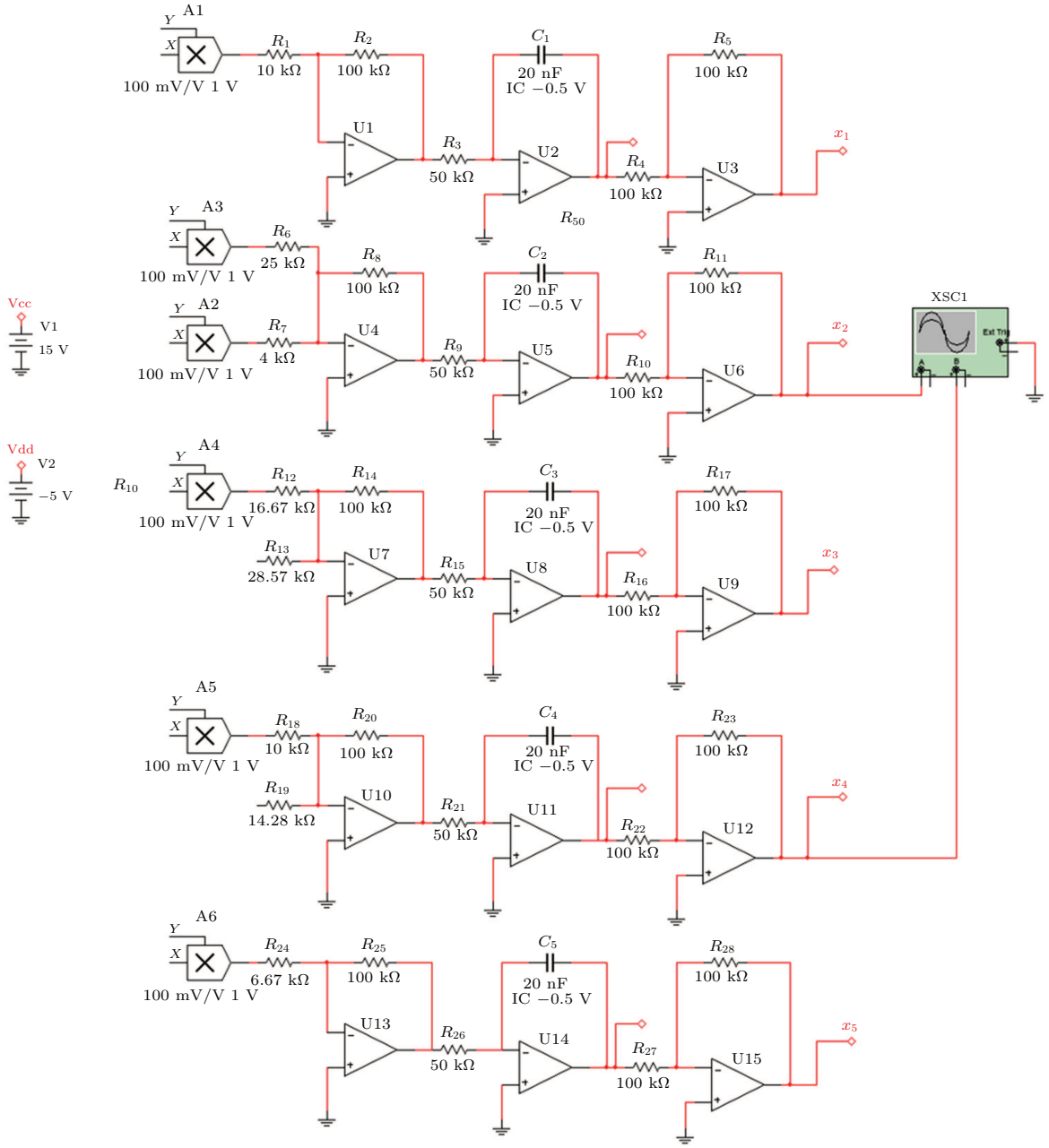


Fig. 14. Multisim circuit diagram of system Σ^H.

$$\dot{x} = \begin{bmatrix} \dot{x}_1 \\ \dot{x}_2 \\ \dot{x}_3 \\ \dot{x}_4 \\ \dot{x}_5 \end{bmatrix} = \begin{bmatrix} 0 & -5x_3 & -5x_2 & 0 & 0 \\ 2x_3 & 0 & 2x_1 & 12.5x_5 & 12.5x_4 \\ 3x_2 & 3x_1 & 0 & 3.5 & 0 \\ 0 & -5x_5 & -7 & 0 & -5x_2 \\ 0 & -7.5x_4 & 0 & -7.5x_2 & 0 \end{bmatrix} \begin{bmatrix} x_1 \\ x_2 \\ x_3 \\ x_4 \\ x_5 \end{bmatrix}$$
$$= \begin{bmatrix} -10x_2x_3 \\ 4x_1x_3 + 25x_4x_5 \\ 6x_1x_2 + 3.5x_4 \\ -10x_2x_5 - 7x_3 \\ -15x_2x_4 \end{bmatrix}. \quad (32)$$

According to Eqs. (29) and (30), its Hamiltonian energy function satisfies

$$\frac{\partial H_*(x)}{\partial x_1}(-10x_2x_3) + \frac{\partial H_*(x)}{\partial x_2}(4x_1x_3 + 25x_4x_5) + \frac{\partial H_*(x)}{\partial x_3}(6x_1x_2 + 3.5x_4) + \frac{\partial H_*(x)}{\partial x_4}(-10x_2x_5 - 7x_3) + \frac{\partial H_*(x)}{\partial x_5}(-15x_2x_4) = 0. \quad (33)$$

Solving Eq. (33) yields the following energy function expression:

$$\dot{H}(\mathrm{x}) = 7x_1^2 + 10x_2^2 + 5x_3^2 + 2.5x_4^2 + 15x_5^2. \quad (34)$$

A modular circuit is designed according to Eq. (28) (see Fig. 14). The corresponding circuit state equation is

$$\begin{cases} \dfrac{\mathrm{d}x_1}{\mathrm{d}t} = -\dfrac{R_3}{R_1R_4C_1}x_2x_3, \\ \dfrac{\mathrm{d}x_2}{\mathrm{d}t} = -\dfrac{R_8}{R_5R_9C_2}(-x_1)x_3 - \dfrac{R_8}{R_6R_9C_2}x_4(-x_5), \\ \dfrac{\mathrm{d}x_3}{\mathrm{d}t} = -\dfrac{R_{12}}{R_{10}R_{13}C_3}(-x_1)x_2 - \dfrac{R_{12}}{R_{11}R_{13}C_3}(-x_4), \\ \dfrac{\mathrm{d}x_4}{\mathrm{d}t} = -\dfrac{R_{16}}{R_{14}R_{17}C_4}x_2x_5 - \dfrac{R_{16}}{R_{15}R_{17}C_4}x_3, \\ \dfrac{\mathrm{d}x_5}{\mathrm{d}t} = -\dfrac{R_{18}}{R_{19}R_{22}C_5}x_2x_4. \end{cases} \quad (35)$$

Now, we compare the coefficients of Eq. (28) with the coefficients of Eq. (33), set the corresponding resistance and capacitance values, at the same time, select 100 mV/1 V as the output scale coefficient of the analog multiplier, and further we set the initial voltages of the five capacitors to be 0.5, 0.1, 0.1, 0.1, and 0.5 V, respectively, corresponding to the initial values of the chaotic system. We select the power supply voltage by using Multisim software for circuit simulation. The simulation results are shown in Fig. 15, and they are consistent with the experimental results in Fig. 2, which proves that the system is a conservative hyperchaotic system without attractors and has superior ergodicity.

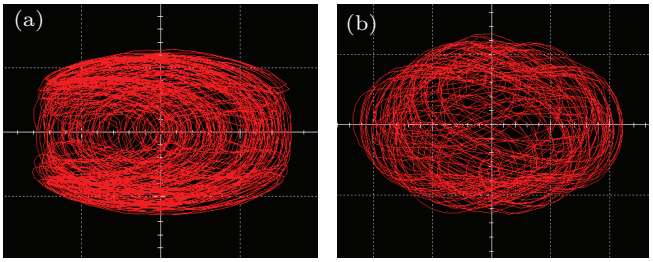


Fig. 15. Circuit simulation diagram of system Σ^H in (a) x_2–x_4 plane and (b) x_3–x_4 plane.

7. Implementation of DSP hardware platform

Hardware implementation is of great significance in studying chaotic systems. Owing to the advantages of DSP digital signal processor such as fast processing speed, strong programmability, and high anti-interference, in this work, the DSP digital signal processor is selected for hardware implementation of the new system.

In our experiment, we first select a digital signal processing chip with a model of TMS320F28335. Then, we discretize the new system based on improved Euler algorithm to obtain the discretized mathematical model, and write the model into the chip in C language. We connect the simulator XDS100-V1 to the computer and utilize a 32-bit 4-channel DAC module with the chip of TLV5620 chip to output chaotic signals. Finally, we set the parameters $(\Pi_1, \Pi_2, \Pi_3, \Pi_4, \Pi_5, a) = (14, 20, 10, 5, 30, 0.7)$, initial values $(x_{10}, x_{20}, x_{30}, x_{40}, x_{50}) = (0.5, 0.1, 0.1, 0.1, 0.5)$, and use the oscilloscope VOS-620B to observe the result (see Fig. 16). Figure 16 shows that the chaotic signal generated by DSP coincides with the Matlab simulation results in Fig. 2(a) under the same system parameters and initial values, realizing the digitization of the chaotic system and proving the physical realizability of the new system.

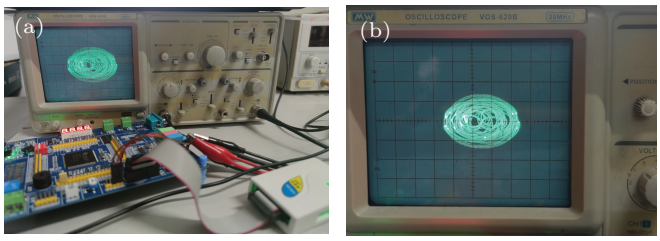


Fig. 16. Hardware implementation of system Σ^H showing (a) DSP experimental platform and (b) chaotic signal generated by DSP in x_2–x_4 plane.

8. Conclusions

Based on the 5D Euler equation, a novel 5D Hamiltonian conservative hyperchaotic system is constructed in this work. By analyzing Hamilton energy and Casimir energy, it is proved that the new system satisfies Hamilton energy conservation and can generate chaos. At the same time, the system has a variety of complex dynamic characteristics, such as time reversal symmetry, wide parameter range, multiple stability. The study of time reversal symmetry plays an important role in solving some physical problems such as quantum mechanics. Chaotic systems have stronger stability and better encryption performance in a wide parameter range. The new system can generate multiple coexisting chaotic orbits under different initial conditions and has good symmetry, revealing

the hidden multi stability dynamics characteristics of the system. Multi stability can be used to process image or generate different random signal sources for application in the field of information engineering. In addition, the conservative and chaotic characteristics of the system are verified through the analysis of divergence, phase diagram, equilibrium point, Lyapunov exponents, and bifurcation diagram. Secondly, through SE complexity analysis and NIST testing, it is proved that the chaotic sequence generated by the new system has high complexity and good pseudo randomness. Finally, using Multisim software and digital signal processor (DSP) to conduct circuit simulation and hardware circuit experiments on a conservative hyperchaotic system, it is confirmed that the new system has good ergodicity and realizability.

Acknowledgements

Project supported by the Heilongjiang Province Natural Science Foundation Joint Guidance Project, China (Grant No. LH2020F022) and the Fundamental Research Funds for the Central Universities, China (Grant No. 3072022CF0801).

References

[1] Tutueva A V, Karimov T I and Moysis L 2021 *Nonlinear Dyn.* **104** 727
[2] Li C, Lin D and Lü J 2018 *IEEE MultiMedia* **25** 46
[3] Lorenz E N 1963 *J. Atmos. Sci.* **20** 130
[4] Chen G R and Ueta T 1999 *Int. J. Bifurc. Chaos* **09** 1465
[5] Lü J H and Chen G R 2002 *Int. J. Bifurc. Chaos* **12** 659
[6] Eisaki H, Takagi H and Cava R J 1994 *Phys. Rev. B* **50** 647
[7] Lü J H, Chen G R and Zhang S C 2002 *Int. J. Bifurc. Chaos* **12** 1001
[8] Mahmoud E E 2012 *Math. Comput. Model.* **55** 1951
[9] Molaie M, Jafari S and Sprott J C 2013 *Int. J. Bifurc. Chaos* **23** 1350188
[10] Wang G Y, Yuan F, Chen G R and Zhang Y 2018 *Chaos* **28** 013125
[11] Dang X Y, Li C B, Bao B C and Wu H G 2015 *Chin. Phys. B* **24** 050503
[12] Tian H, Wang Z and Zhang P 2021 *Complexity* **2021** 8865522
[13] Li C, Sprott J C and Hu W 2017 *Int. J. Bifurc. Chaos* **27** 1750160
[14] Pham V T, Volos C and Jafari S 2016 *Nonlinear Dyn.* **87** 2001
[15] Zhang Z and Huang L 2022 *Nonlinear Dyn.* **108** 637
[16] Ji'e M, Yan D, Sun S and Zhang F 2022 *IEEE Trans. Circuits Syst.* **69** 3328
[17] Ojoniyi O S and Njah A N 2016 *Chaos Solitons Fractals* **87** 172
[18] Bao B C, Jiang T, Xu Q and Chen M 2016 *Nonlinear Dyn.* **86** 1711
[19] Sprott J C, Jafari S and Khalaf A J M 2017 *Eur. Phys. J. Spec. Top.* **226** 1979
[20] Jia H Y, Chen Z Q and Yuan Z Z 2009 *Acta Phys. Sin.* **58** 4469 (in Chinese)
[21] Liu J M and Zhang W 2013 *Optik* **124** 5528
[22] Xu C B and Li Z 2019 *J. Zhejiang University* (*Eng. Sci.*) **53** 1552 (in Chinese)
[23] Bogoyavlensky O I 1984 *Commun. Math. Phys.* **95** 307
[24] Bouteghrine B, Tanougast C and Said S 2021 *J. Circuits, Syst. Comput.* **30** 2150280
[25] Lin Z, Wang G and Wang X 2018 *Nonlinear Dyn.* **94** 1003
[26] Qi G Y 2018 *Nonlinear Dyn.* **95** 2063
[27] Dong E Z, Jiao X D, Du S Z, Chen Z Q and Qi G Y 2020 *Complexity* **2020** 4627597
[28] Qi G Y and Zhang J F 2017 *Chaos Solitons Fractals* **99** 7
[29] Cang S and Wu A G 2018 *Int. J. Bifurc. Chaos* **28** 1850087
[30] Roberts J A and Quispel G R 1992 *Phys. Rep.* **216** 63
[31] Lamb J S and Roberts J A 1998 *Physica D* **112** 1
[32] Sprott J C 2015 *Int. J. Bifurc. Chaos* **25** 1550078
[33] Wolf A, Swift J B, Swinney H L and Vastano J A 1985 *Physica D* **16** 285
[34] Muthuswamy B 2010 *Int. J. Bifurc. Chaos* **20** 1335
[35] Wang N, Zhang G and Kuznetsov N 2021 *Commun. Nonlinear Sci.* **92** 105494
[36] Zhang S, Wang X and Zeng Z 2020 *Chaos* **30** 053129
[37] Zhang S, Li C B and Zheng J H 2021 *IEEE Trans. Circuits Syst.* **68** 4945
[38] Sun K, He S and He Y 2013 *Acta Phys. Sin.* **62** 010501 (in Chinese)
[39] Rukhin A, Soto J, Nechvatal J, Smid M, Barker E, Leigh S, Levenson M, Vangel M, Banks D, Heckert A, Dray J and Vo S 2010 *J. Res. Natl. Inst. Stan.* **800** 22
[40] Hu J B, Qi G Y, Wang Z and Chen G R 2021 *Int. J. Bifurc. Chaos* **31** 2130007
[41] Wang J, Yu W and Wang J 2019 *Int. J. Circ. Theor. Appl.* **47** 702